Calculating Aerodynamic Forces for Bermuda Sail Plans

Copyright © **Ulrich Remmlinger**, Germany, 2023

Abstract. The paper describes the choice of a computational method to calculate the sail forces for a sail plan with head- and mainsail. An optimizer searches for the best trim. The computer code is validated and some example results are presented.

NOMENCLATURE

AR	aspect ratio s/c	w_i	induced velocity normal to chord
c	chord length, distance from luff to leach	x	coordinate parallel to centerline aftwards
C_D	drag-force / ($q{\cdot}c{\cdot}s$) parallel to V_∞	y	coordinate from gooseneck to leeward
C_L	lift-force / ($q{\cdot}c{\cdot}s$) vertical to V_∞ and span	z	from gooseneck parallel to mast upward
d	gap between sail foot and deck	α	geometric angle of attack
D	weight displacement	α_i	induced angle of attack
GM	metacentric height	α_{eff}	effective angle of attack
q	dynamic pressure = $\rho/2{\cdot}\, V_\infty^2$	γ	sheeting angle
Re	Reynolds-number = $V_\infty{\cdot}c/v$	φ	heel angle
RM	righting moment	φ_{VS}	angle of vanishing stability
s	sail-span foot to head, normal to flow	ρ	density of air = 1.225 kg/m^3 (stand. atm.)
V_∞	apparent wind speed far ahead of sail	v	kinematic viscosity of air = 1.461${\cdot}10^{-5}$ m^2/s
V_{eff}	effective wind speed at sail section	ω	Küchemann's correction factor for AR
u_i	induced velocity parallel to chord	Γ	strength of spanwise vortices

1 INTRODUCTION

The aim of my work is the performance improvement of sailing yachts. Part of this task is the optimization of the geometry of the sail plan. This includes not only the sail dimensions but also the trim parameters like sheeting angle, twist and draft at different heights. Since the number of possible combinations is almost infinite, one would prefer to do the trial and error with a computer instead of doing it on the water. The computational methods in use are either fast VPPs, that use simple physical models or on the opposite sophisticated CFD-programs. A typical VPP is the one employed by the ORC [1]. It uses global, empirically determined coefficients to calculate the force developed by an individual sail, based on the apparent wind angle at a predetermined height. It is assumed that this force can be achieved by an optimal trim. The values of the trim parameters remain unknown. For my desired optimization, this method is neither sensitive nor detailed enough. On the other hand, the CFD-methods require a 3D computational mesh of varying density that needs to be modified for every small change of the trim parameters. This is so complex and time consuming, that an automated optimization is not feasible. Instead, a method is needed, that gives a detailed insight into the local flow vectors and local forces across the sail, including the interaction of jib and main. The method must allow an easy change of the geometric dimensions and trim parameters and it must be possible to incorporate this program into an available optimization routine. I will explain the choices that were made, but I will keep the analysis short. If a detailed description of the applied methods is given in the referenced sources, I will not repeat it.

2 THE COMPUTATION METHOD

2.1 Available Methods

The computational methods that are described by Katz & Plotkin [2] meet the above requirements. The lifting-line method, the vortex-lattice method and the panel method are available for three-dimensional numerical solutions of potential flow problems. The lifting-line method divides the wing or sail in the spanwise direction into a large number of elements. A horseshoe vortex is placed on each element, with its bound vortex on the quarter chord line and with its trailing vortex lines parallel to the flow. In the vortex lattice method, a thin lifting surface is not only divided in the spanwise direction into panels, but also in the chordwise direction. A vortex ring is placed on each panel. Wake panels are attached to the trailing edge. This method forces the airflow to follow the contour of the wing all the way to the trailing edge. The so called panel methods add additional panels on both sides of a thick wing and on the fuselage. This way the potential flow around arbitrary thick lifting bodies can be calculated. If the flow is attached and the viscous effects are limited to the very thin boundary layer, it is appropriate to assume that the flow follows the surface of the body. For most airplanes this is the case. Sails are different. Except at the very close-hauled condition, sails exhibit at least partly flow separation, as

demonstrated in [3] for 2D sail sections. Figure 1 depicts the streamlines around a wing section with separated flow. If one would use the vortex lattice method it would be wrong to force the flow to follow the contour of the wing. Instead, one would have to prescribe the streamline that divides the inner separated flow region from the outside potential flow. Since this dividing streamline is unknown, the vortex lattice and the panel methods cannot be used. It is best to use the lifting-line method and to take care of the separation by using the appropriate coefficients for lift and drag. These coefficients can be determined in advance for the 2D sail sections [3].

Figure 1. separated flow behind a wing section
Photo: DLR, 1915, CC-BY 3.0

2.2   The Lifting-Line Solution

Prandtl's integrodifferential equation can be written in a form that is defining an effective angle of attack [2]:

$$\alpha_{eff} = \alpha - \alpha_i \qquad \text{where} \qquad \alpha_i = \frac{w_i}{V_\infty} \tag{1}$$

This equation must be solved for each panel. α is the geometric angle of attack and α_i is calculated from the downwash w_i that is induced by all other vortex lines in the flow area at a control point inside the panel. The velocity at this control point, induced by a vortex line, can be calculated with the use of the subroutine VORTEX as published in [2]. The summation of all induced velocities at the control point must include the trailing vortex lines of all panels of the headsail as well as of the mainsail, of the pieces of the bound vortices on each panel, again on the head- and mainsail and of the same system of horseshoe vortices that is created by the mirror images that simulates the reflection at the water plane. The component normal to the sail chord of this summation will deliver w_i and the induced angle α_i. Subtracting this angle from the geometric angle of attack yields the effective angle of attack. According to Prandtl's hypothesis, a section of the finite wing will produce the same lift as a section of an infinite wing with same profile and effective angle of attack. The lift and drag coefficients can therefore be taken from the 2D-sections [3]. This hypothesis is justified for wings of large aspect ratio, with the exception of their tip regions. The local vortex strength at each panel is calculated from:

$$\Gamma = \tfrac{1}{2} V_\infty \cdot C_L \cdot c \tag{2}$$

The vortex strength can then be used to calculate the downwash as described above. In Prandtl's original form the solution is limited to small angles of attack, where the lift C_L is a linear function of α_{eff}. In this case, the integrodifferential equation is linear and the division into panels transforms it into a system of linear equations. This system can be solved by simple matrix inversion [2]. Katz & Plotkin [2] place the bound vortex line at the quarter-chord line and the control point on the three-quarter-chord line. In this case, the distance between the two points is half a cord length and the bound circulation of the panel can be calculated from Biot-Savart's law:

$$\alpha_{eff} = \frac{w_{eff}}{V_\infty} = \frac{\Gamma}{2 \cdot \pi \cdot V_\infty \cdot \frac{c}{2}} \qquad \text{only valid if} \quad C_L = 2 \cdot \pi \cdot \alpha_{eff} \quad \text{and} \quad AR \to \infty$$

α_{eff} is inserted into eq. 1. This restriction of C_L to its theoretical value is not necessary. It is better, to calculate the downwash at the control point without the inclusion of the bound vortex of its own panel and to calculate Γ separately from eq. 2. In this case, it is possible to take C_L from the tabulated data of 2D-sections [3] and one is free in the choice of the position of the lifting-line and of the control point. The impact of these positions will be discussed later. For sails, the original method needs a modification, because neither is the lift-curve linear nor is the aspect ratio large enough.

2.3   A Modified Lifting-Line Method

Küchemann [4] developed an extension of Prandtl's method to wings with small aspect ratio and sweep. He introduced a factor ω that corrects the results for the movement of the aerodynamic center. For an infinite aspect ratio and attached flow, the aerodynamic center is at the ¼ - chord line. It moves forward to the leading edge of the wing as $AR \to 0$. His factors modify the induced downwash as well as the lift coefficient to include this 3D-effect.

www.remmlinger.com

Next, the right position of the control point must be chosen. The following consideration might help. There are two wings, or two sails, which influence each other. The rules from biplane theory [5] apply in this case. If the circulation on both wings is the same, it follows from Biot-Savart's law, that the induced velocity on each wing will also be the same just the sign is inverted. If the bound vortices were placed at the ¼ - chord line and the control points at the ¾ - chord line, the induced velocity on the rear wing would be significantly less than that on the forward wing, because the distance between vortex and control point would be much larger for the rear wing. This would be physically wrong. Prandtl places therefore the vortex and the control point in the same position. If this rule is obeyed, it is of only minor importance, if the chosen position is 20% or 40% behind the leading edge. The distance between the point on the headsail and the one on the mainsail is in both cases nearly equal, both points are just shifted a similar amount in the flow-direction. The XFOIL-calculations [3] showed that the aerodynamic center lies for many sail sections typically 33% behind the leading edge. We will therefore fix both the bound vortex and the control point at this position. The factor ω corrects the error introduced by considering this position as fixed for all aspect ratios.

Another input from biplane theory is the recognition of the effect of streamline curvature [6]. The onflow to the mainsail is not an undisturbed parallel flow, instead it is a superposition of the parallel flow and the circulation of the headsail and therefore the streamlines are curved. The induced velocity describes a circle around the lifting-line of the headsail. If the mainsail were supposed to produce no lift, it would have to have a camber that follows the streamline. If the mainsail were a flat plate, it would already produce a lift even at zero angle of attack, just because of the streamline curvature. The effective camber of the mainsail is therefore larger than the geometric camber and the mainsail creates an additional incremental lift. The additional fictitious camber can be calculated from the radius of the circulation around the headsail at the control point of the mainsail. The curvature of the circle must be multiplied with u_i/V_∞ because only the streamline curvature in the direction of the chord has an influence (see figure 2). The increase in lift is in the order of 5%. At the headsail, the conditions are inverted and the lift is reduced.

Küchemann's correction factors require the input of the aspect ratio of the sails. The sails are not sealed to the water plane, instead there is a gap. The effective aspect ratio is therefore different from the geometric aspect ratio. Prandtl [5] published an equation that relates these two values to the gap d/s:

$$\frac{AR_{eff}}{AR_{geo}} = 2 - \frac{1}{\sqrt{1 + 0.35 \cdot \left[\log_{10}\left(1 + \frac{s}{d}\right)\right]^2}} \tag{3}$$

Experiments by Munk & Cario [7] revealed that for very small gaps as they appear between the jib foot and deck, viscous effects restrict the flow through the gap. In this case, equation 4 replaces equation 3. If there is no gap, the sail is reflected at the deck and water plane. Together with this mirror image, the effective aspect ratio has twice the value of the geometric aspect ratio of the sail.

$$\frac{AR_{eff}}{AR_{geo}} = \frac{2}{8.064 \cdot \dfrac{d}{d+s} + 1} \qquad\qquad \frac{d}{d+s} \leq 0.092 \tag{4}$$

The next modification is necessary, because the induced velocity at each panel has not only the component w_i normal to the chord but also a component u_i in the direction of the chord. u_i is too large to be ignored. According to figure 2, the vector of the airflow at the local sail section can be described by the angle of attack α_{eff} and by the effective wind speed V_{eff}. In equation 2 V_{eff} must replace V_∞.
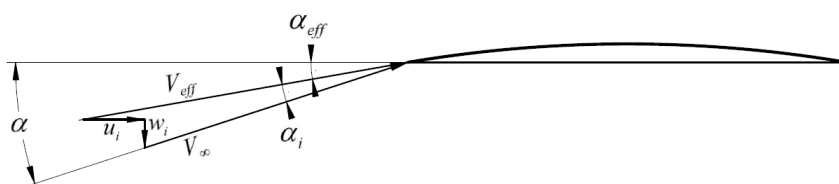

Figure 2. local induced velocities at the sail section w_i and u_i drawn in the positive direction.

Written as a sum of vectors we get:

$$\vec{V}_{eff} = \vec{V}_\infty + \vec{u}_i + \vec{w}_i \quad \rightarrow \quad \tan(\alpha_{eff}) = \frac{V_\infty \cdot \sin(\alpha) - w_i}{V_\infty \cdot \cos(\alpha) + u_i} \quad V_{eff} = \sqrt{V_\infty^2 + u_i^2 + w_i^2 + 2 \cdot V_\infty \left[u_i \cdot \cos(\alpha) - w_i \cdot \sin(\alpha) \right]} \quad (5)$$

Another modification is required, because the lift-curve of sails is highly nonlinear. Figure 3 proves this. Instead of simply inverting a matrix, we now must solve a set of nonlinear equations numerically. A parameter must be chosen, that is updated with each iteration step until convergence. We need a global method that starts with an initial guess and converges reliably to the solution. Phillipps & Snyder [8] chose the lift coefficient and varied the circulation. For the nonlinear regime, they describe the convergence as being slow and the sensitivity to the initial estimate of the circulation as being high. They report only results for the linear part of the lift-curve. Dias [9] also uses the lift coefficient, but in an implicit definition. He calculates C_L from the theoretical position of the separation point and varies this position until convergence. This choice limits the prediction to separated flows. Graf et al. [10] investigated a single wing of large aspect ratio without sweep and used the induced downwash for the iteration. For my work with the problem of two interacting sails, the induced velocities u_i and w_i are the selected parameters that are updated with each iteration step. The method of choice for the numerical task is Broyden's algorithm [11]. The head- and mainsail are each divided into 31 panels, applying a cosine distribution. 124 values for the w_i and u_i are guessed at the initial input to the algorithm and will represent the result after convergence.
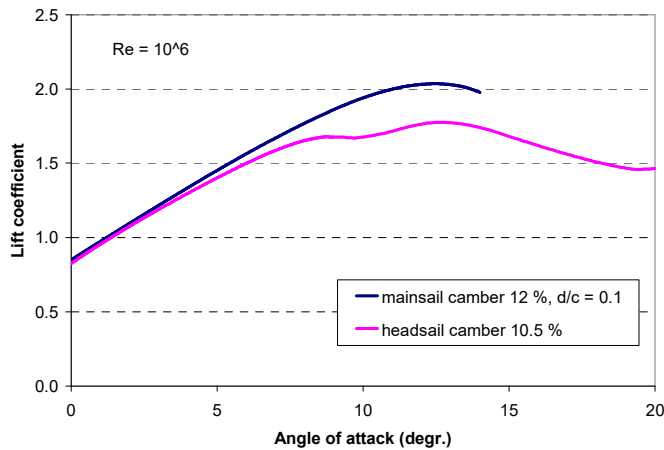

Figure 3. lift-curve for sail sections
calculated with XFOIL [3]

A further problem, caused by the nonlinearity, is the occurrence of solutions with spanwise spikes or even oscillations of the induced velocities. Since different angles of attack can lead to the same lift coefficient, the converged solution is not unique. Neighboring panels can have significantly different induced velocities, angles and lift coefficients. This is a well-known phenomenon [12]. The oscillating velocities are a mathematically valid and converged solution, but they are physically impossible, because viscous effects would smooth out the strong gradients. An improvement can come from a restart with new initial values, which are gained from the oscillating solution by eliminating the spikes. Another possibility is to fit a third order polynomial to the
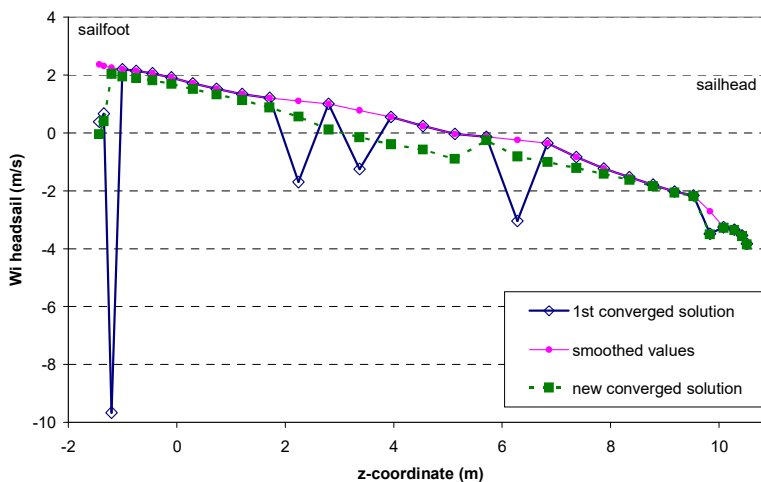

Figure 4. downwash at headsail, impact of smoothing
windspeed 5 m/s, true wind angle 75°

oscillating velocities and use these smoothed values for the new start. Both methods will be used to get a result as realistic as possible. Figure 4 shows the process. The first converged solution for the downwash at the headsail exhibits several spikes; one is severe. Smoothing this result eliminates these spikes and creates a new set of initial values. With these new initial values, the algorithm is started again and the new converged result has no severe spikes. The downwash at the sail head is negative (upwash), because it is under the influence of the strong bound vortex of the mainsail.

2.4   Vortex Lift

Locke et al. [13] measured in the wind tunnel strong vortex cores at the foot of the sails. These vortices create a lift force on the suction side of the sail. Lamar [14] applied the leading-edge-suction analogy to the flow around the side edges of a wing. His equations are also applicable to sails. The vortex lift will increase the lift force for typical sails by approximately 4%.

2.5   The Equilibrium of Moments

A phenomenon that is not covered by the classical lifting-line method is the effect of heel on the flow. All velocities are divided into their components and only the component in the direction of the onflow and the component normal to the onflow and the mast, respectively the forestay, are taken. The component in the direction of the span has no effect and is ignored. It is necessary to prescribe the heeling angle to calculate these components. Having a converged solution one can calculate the sail forces and the heeling moment. This heeling moment has to be compared to the righting moment of the hull at the prescribed heeling angle. If there is a difference, the whole computation must be repeated with an updated guess for the heeling angle. Brent's method [15] is used for this one-dimensional search. The righting moment of the hull is approximated by:

$$RM = \sin(\varphi) \cdot \cos\left(\varphi \cdot \frac{90°}{\varphi_{VS}} \right) \cdot \overline{GM} \cdot D \tag{6}$$

φ_{VS} is the angle of vanishing stability. It can be calculated from the formulae in [16]. GM is the distance from the center of gravity to the metacenter. This righting moment will increase, if there are crewmembers on the rail.

3   THE INDEPENDENT VARIABLES

A large number of independent variables is necessary to fully describe the geometry of the sails and the aero-dynamic influence of the hull. Whether a sail is reefed or not is contained in the specified dimension of the sail. It is desirable to use for the trim of the sails not more parameters than necessary. This will reduce the workload for the optimization. For the mainsail the sheeting can be defined by prescribing the sheeting angle γ at the boom and in addition the twist = γ (head) − γ (boom). The camber of the sail is determined from α_{eff}. For each angle, there is an optimal camber that delivers the best lift/drag-ratio [3]. It is assumed, that this camber can be realized, if necessary with a fully-battened main. For the headsail, there is a dependence between camber, sheeting point on deck and angle γ of the chord at the height of the clew [3]. The sheeting point on deck is assumed to lie on the extension of a straight line from the midpoint of the luff to the clew. If the distance of this sheeting point from the centerline of the ship is given and the camber at the clew is prescribed, then the sheeting angle at the clew is fixed. This dependence does not hold, if a whisker pole is used. In this case, it is necessary to prescribe sheeting angle and camber. The camber at the clew defines the maximum draft. The draft as a function of the height above deck is calculated from two quadratic equations that reduce the draft to zero at head and tack and join at the clew. The local camber can then be calculated from camber = draft/chord. The last parameter that is necessary to describe the headsail is its twist.

Additional parameters describe the hull. The sails create an induced pressure on the hull [17]. This induced force and the drag forces on the hull and on the standing rigging must be taken into account.

Another independent variable is the apparent wind vector. The wind speed at 10 meters height and the boat speed are required as input. The profile of the true wind speed as a function of the height above the water must be determined. Bethwaite [18] observed as a sailor the difference between light air that prevails at wind speeds up to 5 knots and a breeze above 5 knots. In light air, the atmospheric boundary layer is laminar and the wind speed increases linearly with the height. In a breeze, the boundary layer is turbulent and the wind speed follows a logarithmic profile. Högström et al. [19] confirmed this observation with measurements in the Baltic Sea and around Hawaii. They found that the linear region reaches up to 8 meters. Above that limit, the wind speed remains constant in light air. The logarithmic profile at higher wind speeds is characterized by the roughness

length z_0. At wind speeds up to 50 knots the drag coefficient, which is a direct function of z_0, can be approximated by a linear dependence on the wind speed [20]. It is therefore sufficient to specify only the wind speed, the profile follows from that.

4   OPTIMIZATION

There are four trim parameters that can be optimized: for the mainsail these are sheeting angle of the boom and twist and for the headsail camber and twist. Since the converged solutions of the nonlinear set of equations are not unique and sometimes they even fail to converge, the solution surface has "holes" and is "rough". For such noisy functions, it is not possible to calculate derivatives. The optimization without derivatives is an active research area [21]. The software IFFCO (Implicit Filtering For Constrained Optimization) [22] is used for this task. The algorithm will minimize a figure of merit. In a first step this is the component of the sail force in the *x*-direction. Without additional constraints, the optimizer will select trim parameters that create an unrealistically large side force. It is therefore necessary to calculate the induced resistance at the keel that is caused by this side force and subtract this drag from the sail force. This will give a driving force that can be optimized. The induced resistance is calculated in this work with the Delft-method [23]. As already described, the solution for the induced velocities will not always be without spikes and sometimes it will be wavy. Such solutions should be avoided. Therefore, a penalty is defined that incorporates the number of spikes and the standard deviation from fourth order polynomials, fitted to the curve of induced velocities. This penalty is used to reduce the driving force which produces an effective figure of merit.

Kelley [21] writes about implicit filtering: "No algorithm…is guaranteed to find even a local minimum, much less a global one." and "One approach to improve the robustness of these algorithms is to restart the iteration..". The result of the iteration depends on the initial values for the trim parameters at the start. Often the result is close to the initial values and not necessarily a global optimum. It is therefore recommended to restart the iteration with a different set of initial values. The results should be compared and checked for plausibility.

5   RESULTS

The algorithms and iterations were coded in Fortran, compiled with the latest Intel® Fortran Compiler Classic and run on a Windows operating system for Intel® 64 architecture. If the trim parameters are fixed, the program runs only seconds. The further optimization of the trim parameters can take an hour.

5.1   Validation

A simple test for Küchemann's extension to airfoils of low aspect ration is the comparison of the predictions with measurements of rectangular flat plates. Mueller [24] published results that are especially suited for this purpose, because he measured the wings and the 2D-version of the wing in the same wind tunnel. It is therefore possible to use the measured section-characteristics as input to the lifting-line prediction, which will then only model the 3D-effects. The results are shown in figure 5.
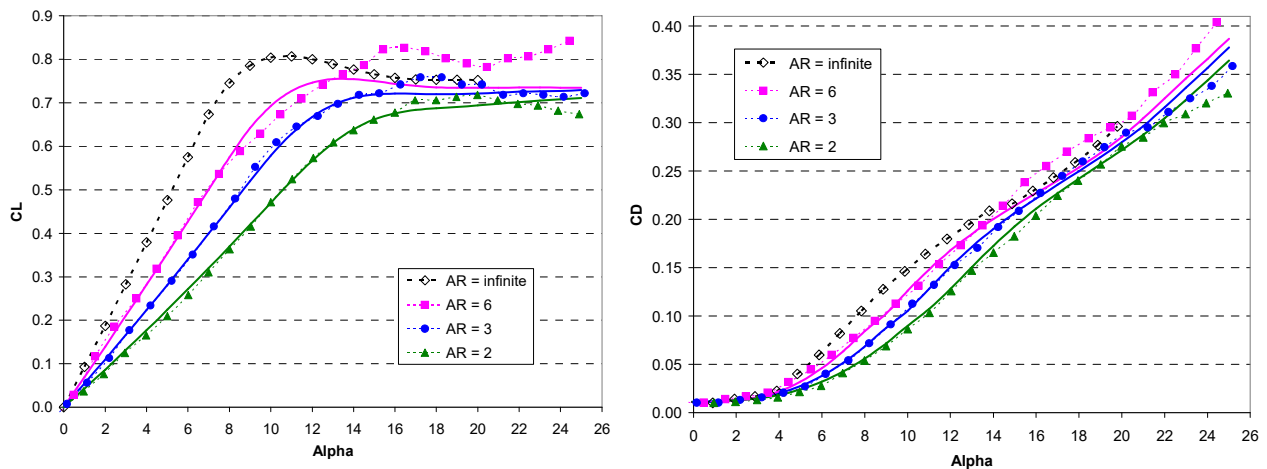

Figure 5. lift and drag coefficients for rectangular flat plates of AR 2-6
symbols represent experiments, solid lines are predictions
Reynolds-number = $1.4 \cdot 10^5$

It is not clear why the measured C_L-values for $AR = 6$ are higher than the 2D-values at the larger angles. This should not be the case. One can only speculate that there is a hysteresis at such low Reynolds-number. As explained in [3] XFOIL predicts a different lift value when the angle is increased compared to the case, when the angle is decreased, coming from a larger value. Such a hysteresis can also happen in the wind tunnel. Apart from this phenomenon, the predictions are good for the angle of attack range without severe flow separation. With Küchemann's modification and Lamar's vortex lift, the lifting-line method is not restricted any more to large aspect ratios. The nonlinearity of the 2D-characteristic was handled without problems. For the fully separated flow at large angles of attack, one cannot expect that Prandtl's hypothesis of the validity of 2D-section charac-teristics still holds. Katz & Plotkin [2] show pictures with surface-oil flow patterns for rectangular wings of aspect ratios from $AR = 3$ to $AR = 12$ and $\alpha = 18.4°$. Several stall-cells develop in the span-wise direction and the width of these cells is almost independent of the aspect ratio. The real flow over the wing sections varies periodically along the span. Mueller used in the test of the 2D-section a plate with a geometric aspect ratio of 1.5 between end walls. The stall cell pattern in the 2D-case was most likely different from the one for the wing with $AR = 6$. This might explain, that the use of this 2D section data produced better agreement at $AR = 2$ than at $AR = 6$. For such complex flows around fully stalled wings, the lifting-line method can only deliver an estimate.

Useful experimental results for the validation of the program with yacht-models in a wind tunnel require the complete information about the geometric dimensions, the sail trim and the wind profile in the tunnel. Such publications are rare. Marchaj [25] measured a Finn-type rig, scaled 1:2.5, where the mast was directly fixed to the wind tunnel floor. For an apparent wind angle of 25°, he listed all the required trim parameters. The lifting-line method yielded the following results:

"run VII"	measured	predicted	error
Lift force	103.1 N	109.6 N	6.4%
Drag force	31.5 N	29.2 N	-7.3%

Marchaj's sail profile resembled a circular arc, whereas the prediction uses a naca-meanline because of its better lift to drag ratio. In addition the sail in the wind tunnel was made of sail cloth with wrinkles. These two effects might explain the lower lift and higher drag in the experiment. The average Reynolds-number was sufficiently large at $5.6·10^5$.

Fossati et al. [26] published results of a model of a 48' IMS yacht at apparent wind angles of 22° and 27° in upright condition. A typical result is listed in the following table:

22° - test no. 12	measured	predicted	error
C_L	1.40	1.337	-4.5%
C_D	0.15	0.180	18.5%

The predicted lift coefficient is acceptable, but the drag coefficient is too large. Fossati subtracted the measured drag of the bare hull and rig from the measured total forces with sails. The value of the subtracted forces was not published and can only be guessed. In addition, the average Reynolds-number was rather low at $1.3·10^5$. It is possible that the boundary-layer was laminar and not turbulent in some areas. This could also reduce the measured drag.

The experiments by Masuyama et al. [27, 28] come with a complete set of the required parameters. The authors measured sail forces on a full size yacht dynamometer and compared the measured values with calculated pre-dictions, using a vortex lattice method and a RANS-based CFD method. The sail shapes were determined with several distributed cameras. Apparent wind angle and wind speed were measured with an anemometer 4.8 meters directly above the bow. This presents a problem, because the position is less than a chord length in front of the jib and the flow is not undisturbed. The circulation around the headsail influences the streamlines and the measured apparent wind angle is about 5° larger than the apparent wind angle very far in front of the boat. It is possible to get a first indication of the induced velocities at the position of the anemometer with the lifting-line method. For the measurement no. 9609233A [27] a true wind angle of 43.4° results in the measured wind angle of 30.9° at the anemometer. With this complete set of input parameters, it was possible to run the lifting-line program. The results are depicted in figure 6. The measured sail forces on port tack differed from the ones on starboard tack. The forces also varied over time between a maximum and minimum value. The diagram shows therefore a band around the mean values for the forces $-Fx$ and Fy. All predictions are too low. The RANS- and

VLM-values were not corrected for the position of the anemometer [28]. The correction would even lower these CFD results and make them worse. Masuyama published several datasets with different sail trims. Some would give a better agreement between measurement und predictions. Picking just the favorable results would be no honest validation.
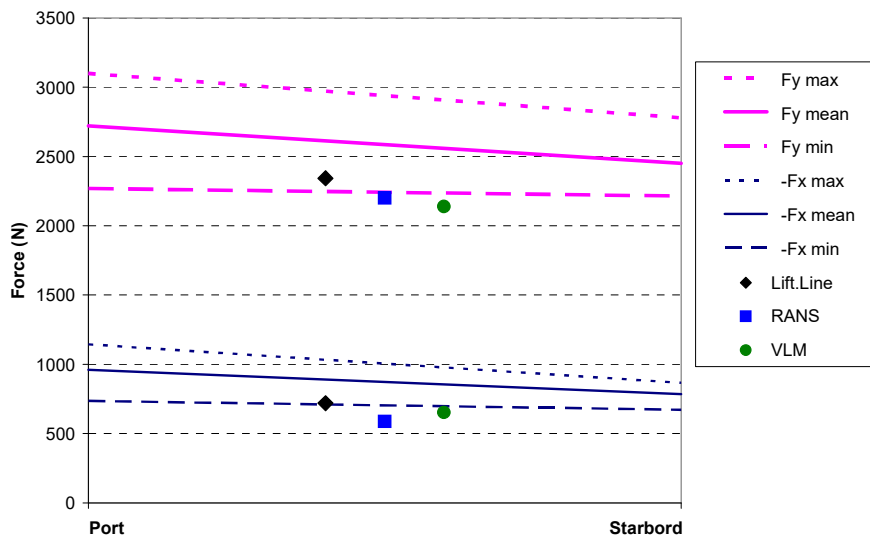

Figure 6. calculated components of the sail force compared with measurements

In summarizing the validation, one can say, that the lifting-line method is a suitable tool to predict the sail forces. The accuracy of the results is as good as those of the CFD methods, but they come at significantly lower computational costs.
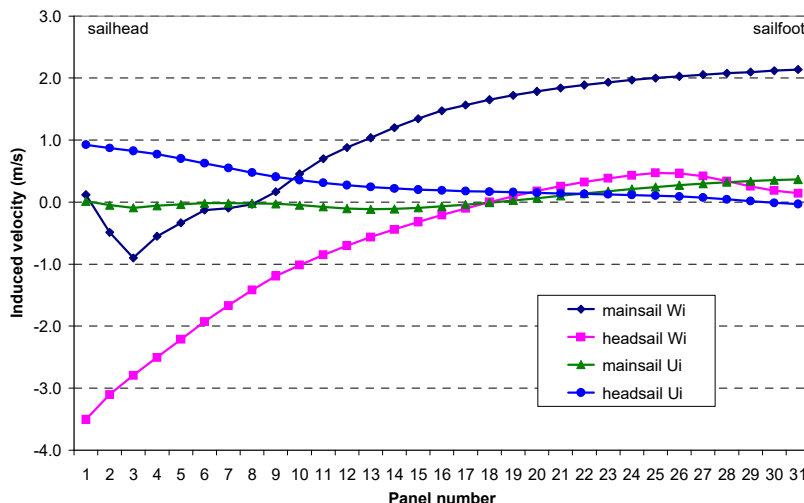
5.2   Examples

Some authors [17] used the Dehler 33 as an example, because the necessary information about the design is available and complete. The following diagrams show results at the ends of the range of possible courses, first at a true wind angle of 40° and then at 135°. The sheeting angle γ is measured between the sail chord and the centerplane. Twist is the difference γ_{top} - γ_{foot}.

independent variables:		optimum found:	
true wind angle	40°	heel angel	26.8°
true wind speed	10 kts	sheeting angle mainsail foot	0°
boat speed	6.1 kts	twist mainsail	14.9°
leeway angle	6.8°	camber headsail at clew	8.8%
jib sheeting angle on deck	10°	twist headsail	20.4°
sail profile	NACA-mean line	driving force	392.8 N

At first, it is necessary to check the distribution of the induced velocities for spikes or oscillations. Here we see smooth curves. The kink of w_i for the mainsail at the top is caused by unreliable 2D-section data. For the first two points xfoil-data is extra-polated beyond $d/c = 0.5$. The error is irrelevant, because the sail chord is so small, that the contribution to the total sail force is negligible.

The following diagrams depict the distribution of the optimized variables along the vertical *z*-coordinate:
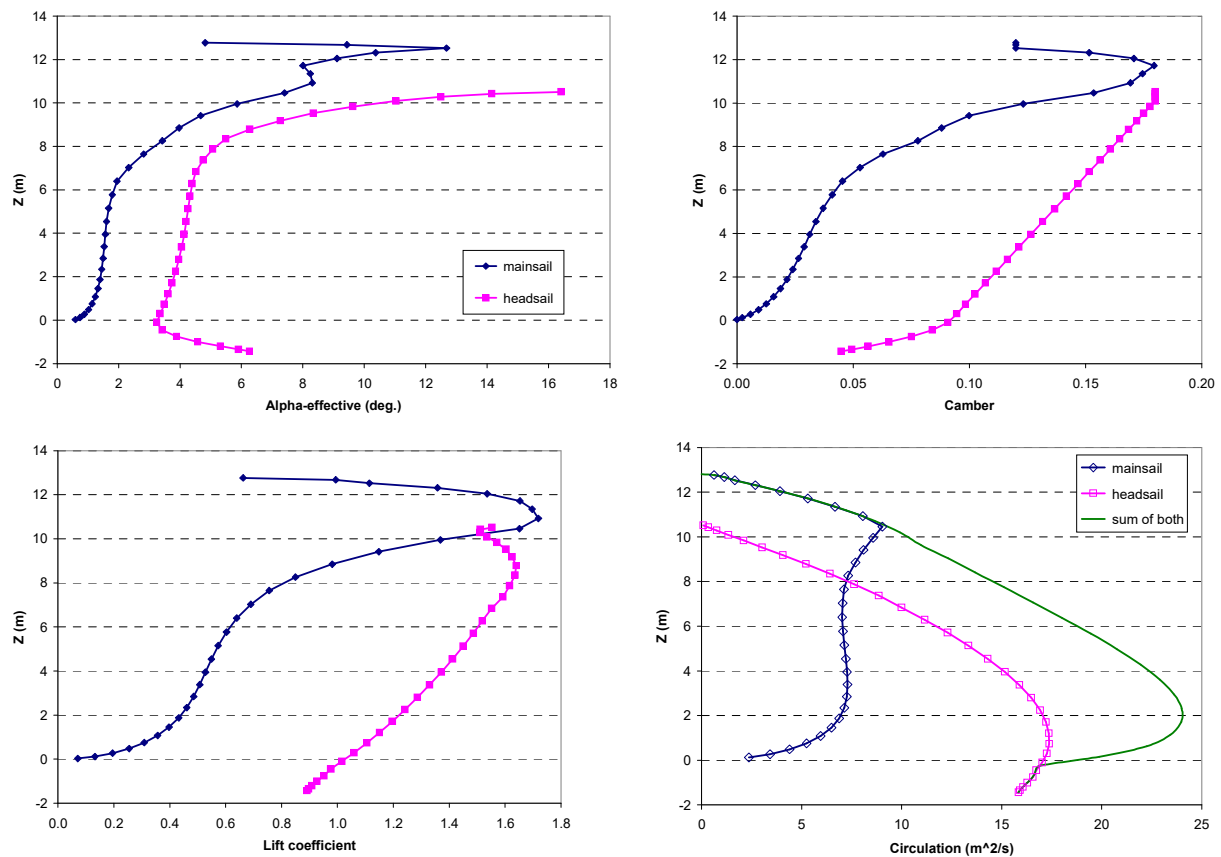

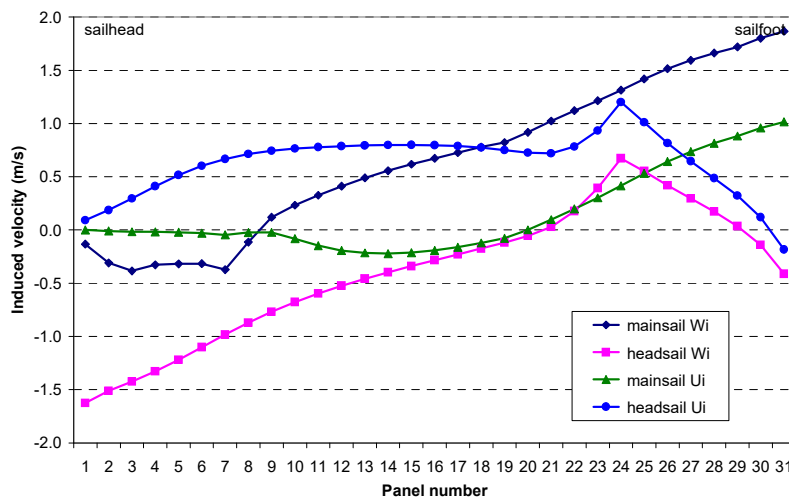
Figure 7. Dehler 33 at TWA = 40°, AWA = 21.5°

It is interesting to note, that the optimizer creates a smooth distribution of the total circulation. The circulation of the mainsail exhibits a sharp kink at the hounds, where the circulation of the headsail starts from zero. The sum of both is smooth. The maximum allowed camber for both sails was limited at 18%.

independent variables:		optimum found:	
true wind angle	135°	heel angel	4.5°
true wind speed	10 kts	sheeting angle mainsail foot	45.5°
boat speed	7.1 kts	twist mainsail	43.9°
leeway angle	1.0°	camber headsail at clew	36%
jib sheeting point	foot-rail	twist headsail	40.4°
sail profile	parabola	driving force	715 N

In the second example, the induced velocities of the headsail show a peak at panel 24, that contains the clew of the jib. There is a sudden change in the sweep-angle at this point, which causes the peak. The high positive values of u_i at the headsail are induced by the bound vortex of the mainsail.
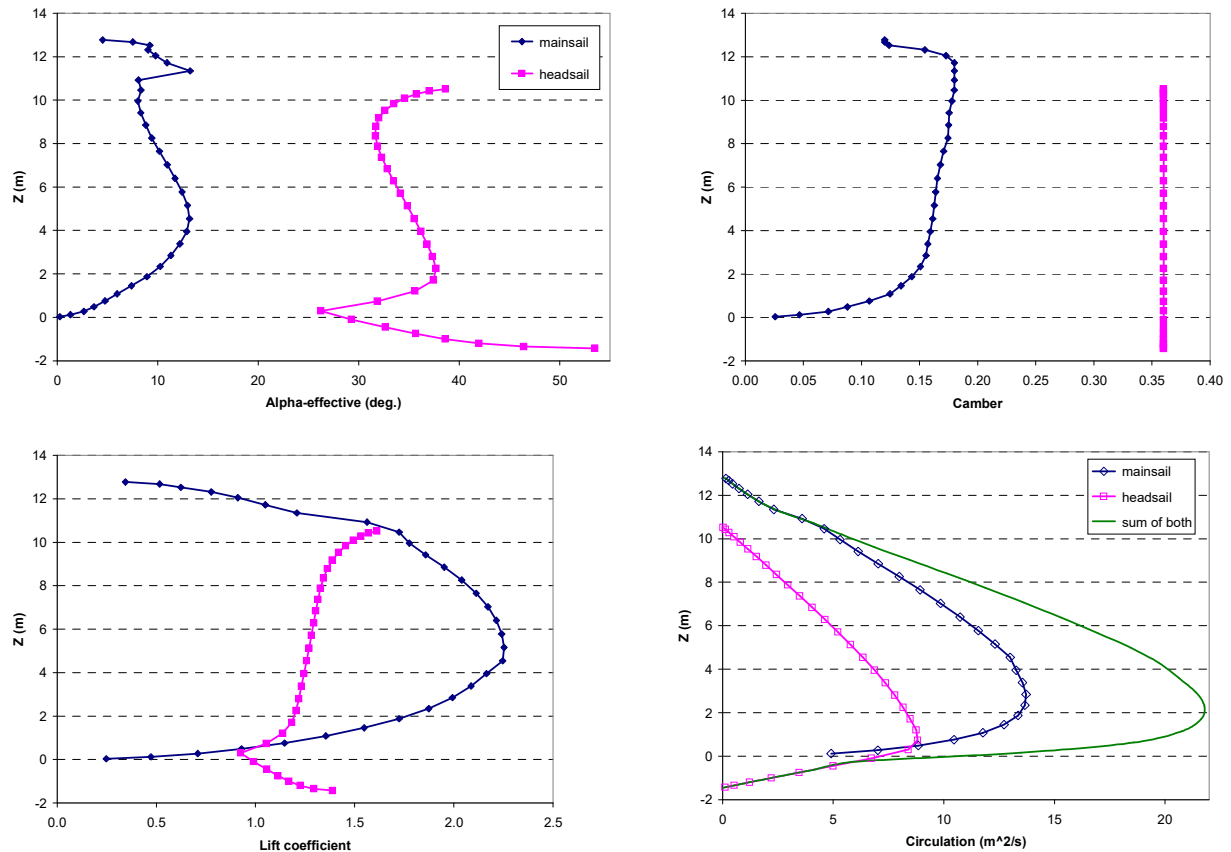
Figure 8. Dehler 33 at TWA = 135°, AWA = 84.7°

In this example, the profile of the headsail follows a parabola and the sheet ran to the foot rail. The maximum camber for the parabolic headsail is 36%. The changeover point from the NACA-profile to the parabola occurs at an apparent wind angle of about 40°. The parabolic sail, sheeted to the foot rail, creates a higher driving force above this value. Without a whisker pole, it is not possible at such large *AWA* to increase sufficiently the sheeting angle of the headsail. The flow over the sail is therefore fully separated. The effective angle of attack is larger than 30°. The algorithm finds a converged solution even for this highly non-linear case. The mainsail generates ⅔ of the circulation. In the first example, sailing close-hauled upwind, the relationship was reversed.

A weak point of the current algorithm is the optimizer. The program finds a good solution, but not necessarily the optimum. The result depends very much on the initial starting values for the trim parameters. It is therefore necessary to run several copies of the program in parallel with different starting values. On today's multi-core machines this is not a problem.

6   CONCLUSION

The lifting-line method is a computational tool that offers fast results for arbitrary sail geometries. The detailed distributions of the flow-parameters allow an insight into the flow conditions at the sails. The calculated sail forces are comparable to the results gained with more expensive methods (CFD). It is possible to identify optimal trim settings, even if the absolute accuracy of the calculated force might not be high. Finding the global optimum for noisy functions is still a research area. It is possible, that more effective algorithms become available in the future. It seems that some commercial codes perform already better than IFFCO [29].

7   REFERENCES

1.   Offshore Racing Congress, *ORC VPP Documentation*, 2022, www.orc.org

2.   Katz, J., Plotkin, A., *Low-Speed Aerodynamics*, Cambridge, UK: University Press, 2001

3.   Remmlinger, U., "Aerodynamic Characteristics of 2D Sail Sections ", [Online]. Available: http://www.remmlinger.com/2D%20aerodynamics.pdf

4. Küchemann, D., "A Simple Method for Calculating the Span and Chordwise Loading on Straight and Swept Wings of any Given Aspect Ratio at Subsonic Speeds", *Aeronautical Research Council, R.&M.* No. 2935, London, 1956

5. Prandtl, L., "Tragflügeltheorie, II. Mitteilung", *Nachrichten der K. Gesellschaft der Wissenschaften zu Göttingen, Mathematisch-physikalische Klasse*, pp. 107-137, 1919

6. Prandtl, L., "Über den Einfluß der Stromlinienkrümmung auf den Auftrieb von Doppeldeckern", *Ergebnisse der Aerodynamischen Versuchsanstalt zu Göttingen*, III. Lieferung, München, Berlin: Oldenbourg, 1927

7. Munk, M., Cario, G., "Flügel mit Spalt in Fahrtrichtung", *Technische Berichte von der Flugzeugmeisterei der Inspektion der Fliegertruppen*, Band 1, pp. 219-222, Berlin, 1917

8. Phillips, W.F., Snyder, D.O., "Modern Adaptation of Prandtl's Classic Lifting-Line Theory", *J. Aircraft*, vol. 37, no. 4, pp. 662-670, 2000

9. Dias, J.N., "Nonlinear Lifting-Line Algorithm for Unsteady Post-stall Conditions", *34th AIAA Applied Aerodynamics Conference*, 2016 Washington D.C.

10. Graf, K., Hoeve, A.v., Watin, S., "Comparison of full 3D-RANS simulations with 2D-RANS/lifting line method calculations for the flow analysis of rigid wings for high performance multihulls", *Ocean Eng.*, vol. 90, pp. 49-61, 2014

11. Broyden, C.G., "A Class of Methods for Solving Nonlinear Simultaneous Equations", *Mathematics of Computation,* vol. 19, No. 92, 1965, pp. 577-593

12. Hunsaker, D.F., "Post stall behavior of a lifting line algorithm", in: *Rocky Mountain Space Grant Consortium Meeting Proceedings*, 2007, Salt Lake City, Utah.

13. Locke, N.J., Jackson, P.S., Flay, R.G.J., "Lift and Drag Distributions of Yacht Sails Using Wake Surveys", *Trans. ASME, J. Fluids Eng.*, Vol. 118, pp. 346-351, 1996

14. Lamar, J.E., "Extension of Leading-Edge-Suction Analogy to Wings with Separated Flow around the Side Edges at Subsonic Speeds", NASA Langley, TR R-428, 1974

15. Brent, R.P., *Algorithms for Minimization without Derivatives*, chapter 4, Englewood Cliffs, NJ: Prentice-Hall, 1973

16. Maritime and Coastguard Agency, *Code of Practice for the Construction..of Sailing Vessels..*, para 11.1.2.4, London, UK: The Stationary Office, 1998

17. Hansen, H., "Enhanced Wind Tunnel Techniques and Aerodynamic Force Models for Yacht Sails", Ph.D. diss., Dept. Mech. Eng., Univ. Auckland, Auckland, New Zealand, 2006

18. Bethwaite, F., *High Performance Sailing*, 2nd ed. London, UK: Adlard Coles, 2010

19. Högström, U., Rutgersson, A., Sahlée, E. *et al.* "Air–Sea Interaction Features in the Baltic Sea and at a Pacific Trade-Wind Site: An Inter-comparison Study", *Boundary-Layer Meteorology* , vol. 147, pp. 139–163, 2013

20. Zhao, D., Li, M., "Dependence of wind stress across an air–sea interface on wave states", *J. Oceanography*, no. 75, pp. 207-223, 2019

21. Kelley, C.T., *Iterative Methods for Optimization*, Philadelphia, Pa.: SIAM, 1999

22. MATLAB-code available: https://ctk.math.ncsu.edu/iffco.html, the FORTRAN-code, used in my work, is no longer available.

23. Keuning, J.A., Sonnenberg, U.B., "Approximation of the Hydrodynamic Forces on a Sailing Yacht based on the DSYHS", *Int. HISWA symposium*, Amsterdam, NL, 1998

24. Pelletier, A., Mueller, T.J., "Low Reynolds Number Aerodynamics of Low-Aspect-Ratio, Thin/Flat/Cambered-Plate Wings", *J. Aircraft*, Vol. 37, No. 5, pp. 825-832, 2000

25. Marchaj, C.A., *Aero-Hydodynamics of Sailing*, London, UK: Adlard Coles, 1979

26. Fossati, F., Muggiasca, S., Martina, F., "Experimental Database of Sails Performance and Flying Shapes in Upwind", in *Proc. Innovation High Performance Sailing Yachts*, Lorient, France, 2008, pp. 99-114

27. Masuyama, Y., Tahara, Y., et al., "Database of sail shapes versus sail performance and validation of numerical calculations for the upwind condition", *J marine science technol.*, vol. 14, no. 2, pp. 137–160, 2009

28. Masuyama, Y., Fukasawa, T., "Full Scale Measurement of Sail Force and the Validation of Numerical Calculation Method", *13ᵗʰ Chesapeake Sailing Yacht Symposium*, SNAME, pp. 23-36, 1997

29. Rios, L.M., Sahinidis, N.V., "Derivative-free optimization: a review of algorithms and comparison of software implementations", *J. Glob Optim*, No. 56, pp. 1247-1293, 2013